

# Further improvement of Pb/Cd-free $\text{CaRuO}_3$ thick-film resistors

(Ulepszone bezołowiowe rezystory grubowarstwowe na bazie  $\text{CaRuO}_3$ )

dr inż. ADAM WITOLD STADLER<sup>1</sup>, mgr inż. ZBIGNIEW ZAWIŚLAK<sup>1</sup>,  
prof. dr hab. inż. ANDRZEJ KOLEK<sup>1</sup>, mgr inż. KONRAD RAFAŁ KIEŁBASIŃSKI<sup>2,3</sup>,  
dr hab. inż. MAŁGORZATA JAKUBOWSKA<sup>2,4</sup>, prof. PW

<sup>1</sup> Department of Electronics Fundamentals, Rzeszow University of Technology, Rzeszow

<sup>2</sup> Institute of Electronic Materials Technology, Warsaw

<sup>3</sup> Warsaw University of Technology, Institute of Microelectronics and Optoelectronics, Warsaw, Poland

<sup>4</sup> Warsaw University of Technology, Faculty of Mechatronics, Warsaw

Thick-film resistors (TFRs) are very popular in many fields of electronics. They are typically made from pastes containing conducting ( $\text{RuO}_2$ ,  $\text{Bi}_2\text{Ru}_2\text{O}_7$  or  $\text{CaRuO}_3$ ) and Pb-containing glass components as well as organic vehicle, which are screen-printed on substrates and then fired in low or high temperature processes. TFRs gained many proponents over years of their usage, due to their advantages, as cheap technology, good performance parameters, and easy control of sheet resistance. On the other hand,  $\text{RuO}_2$ -based resistors enter very demanding field of temperature sensing in cryogenics. Novel technique called printing electronics, in conjunction with eco-friendly materials, opens new page and makes thick-film technology still perspective. However, it implies design of new materials, like Pb/Cd-free solders and pastes for TFRs, what is challenge for technologists who have to develop new generation of materials. For example, well known and widely used in TFRs fabrication  $\text{RuO}_2$ -based resistive pastes include lead-borosilicate glass and therefore they do not fulfill RoHS directive and have to be replaced with their Pb/Cd-free counterparts. Unfortunately, in spite of great effort, Pb/Cd-free TFRs are still at the explorative stage [1–5]. However, first attempts, suggest that  $\text{CaRuO}_3$  better works with Pb/Cd-free glasses [4] and therefore it is more promising conducting component than widely used  $\text{RuO}_2$ . On the other hand, currently Pb/Cd-free  $\text{CaRuO}_3$ -based TFRs are noisier than Pb/Cd-free  $\text{RuO}_2$ -based or Pb-containing TFRs and form bad interface at least with Pb/Cd-free AgPd-based, contacts [6].

In this work we present our new results concerning studies of electrical properties of Pb/Cd-free  $\text{CaRuO}_3$ -based TFRs. The innovation is that the resistive paste was made of the conducting component which is the mixture 1:1 of  $\text{CaRuO}_3$  and  $\text{RuO}_2$  powders. Resistance vs. temperature measurements and low-frequency noise spectroscopy methods have been applied to obtain  $R(T)$  curves and noise maps. The latter were useful to extract parameters describing bulk and contact noise. Next, compatibility of the resistive paste with different conducting pastes has been evaluated.

## Sample preparation

The  $\text{RuO}_2/\text{CaRuO}_3$  mixture with the ratio 1:1 (by weight) has been used as a conducting component for preparation of the resistive paste. Pb/Cd-free glass R-10 of complex composition, which was already used in our earlier studies [6], and an organic vehicle have been added to the above mixture to obtain the resistive paste with 28% (by volume) conducting phase content. The paste was then screen-printed on alumina

substrates, on which metallic contacts made of (also Pb/Cd-free) pastes were previously deposited. After drying, samples were firing in the tunnel furnace using proper temperature profile with peak at 820°C for 8 minutes.

TFRs have been designed as multiterminal devices with the rectangular resistive film of  $w = 1$  mm width and  $L = 15$  mm length and several lateral, evenly spaced, voltage probes. The opposite edges of the resistive film are terminated with current contacts. The picture of the sample resistor and terminations numbering is shown in the inset of Fig. 1. Advantages of such shape of the resistor are described in [6].

For each of the following conducting pastes Ag, AgPd, Ag-AgPt-Pd, several TFRs were prepared. From each series two samples with matched resistance between terminations 1 and 7 ( $R \equiv R_{1-7} = V_{1-7}/I$ , where  $I$  is biasing current and  $V_{1-7}$  is the voltage between terminations 1–7), measured at room temperature, have been selected for noise studies. No ageing treatment has been applied.

Preliminary tests of selected samples cover thickness and voltage distributions measurements in order to calculate sheet resistance  $R_{sq}$  and evaluate influence of contacts. Exemplary plots of thickness and voltage distributions along the resistive layer are shown in Fig. 1.

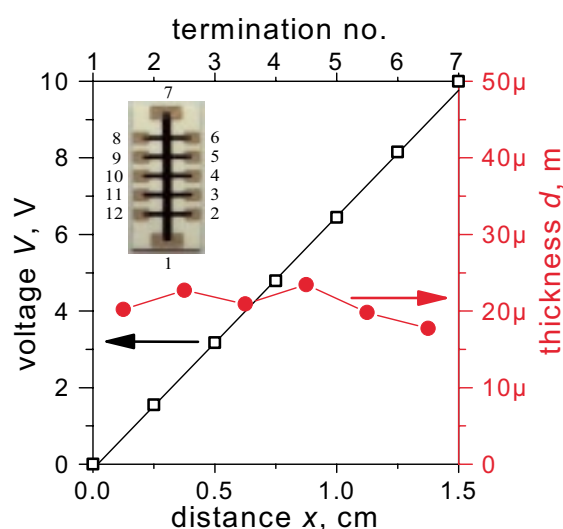


Fig. 1. Voltage (squares) and thickness (solid circles) distributions along the resistive film. The picture of the sample TFR with terminations numbering is shown in the inset  
Rys. 1. Rozkłady napięcia i grubości wzdłuż warstwy rezystywnej. We wstawce pokazano zdjęcie przykładowego rezystora z numeracją końcówek

For all selected samples, sheet resistance  $R_{sq}$  and influence of contacts on it have been evaluated using voltage distribution. Size effect was calculated as the ratio of average resistance per square,  $R_{1-7}w/L$ , and “bulk” sheet resistance  $R_{sq} = V_{2-6}w/(L_{2-6}I)$ , where  $L_{2-6}$  is the length of the sector between contacts 2–6 and  $V_{2-6}$  is the voltage across this sector. Detailed description of samples is given in *Table 1*.

Tabl. 1. Samples description and their parameters at room temperature  
Tab. 1. Opis badanych rezystorów i ich parametry wyznaczone w temperaturze pokojowej

Sample	P-120	P-202	P-511
Contacts	Ag	AgPd	Ag-AgPt-Pd
Thickness $d$ , $\mu\text{m}$	24.3	24.1	25.0
Sheet resistance $R_{sq}$ , $\text{k}\Omega$	2.55	2.60	2.55
resistivity, $\Omega\text{cm}$	6.2	6.25	6.5
Size effect	1.01	1.02	1.02

## Experiment

Noise and resistance measurements were performed in the LN cryostat in temperature range from 77K up to 300K. Advantages of dc bridge method have been taken to reject unwanted common signals (like power supply drift) and dc bias. Two selected samples have been inserted into lower arms of the bridge. Voltages acquired from diagonal and sub-diagonals of the bridge were conditioned in low-noise preamplifiers and low-pass filters and then connected to PC equipped with DAQ board, where digital signal processing has been performed in real time [6]. Additional instruments have been engaged to monitor actual temperature  $T$  and biasing parameters, that makes  $R(T)$  curve measurements possible.

Consecutive noise (cross)spectra were calculated in frequency band from 0.5 Hz to 131072 Hz and averaged over 600 s periods. Only low-frequency part (up to 5 kHz) of the averaged spectra was recorded with actual resistance and temperature.

## Results

### Noise identification

To identify the noise, spectrum shape and its dependence on sample excitation have been examined at room temperature. Typical excess noise spectra  $S_{V_{ex}} = S_V - S_{V=0V}$ , where  $S_V$  ( $S_{V=0V}$ ) is power spectral density (PSD) of voltage fluctuations on terminations 7 measured with bias (with no bias), are shown in *Fig. 2*. Additional data series  $S_{V=0V}$  and reference line  $1/f$  have been added to clarify the plot.  $1/f$  dependence is visible even in the limit of higher frequencies, where background noise is significant at least at low bias voltages. Noise intensity dependence on voltage bias is shown on plot in *Fig. 3*, where  $V^2$  proportionality has been examined. Small spread of noise intensity in different bands at the fixed bias, suggests that noise components other than  $1/f$  also exist. However, linear dependence on voltage square is valid in all tested frequency bands, which is the evidence that all noise components result from resistance fluctuations.

Noise spectra taken for different samples were gathered in the inset of *Fig. 3* and plotted as product of excess noise and frequency vs. frequency in order to emphasize spectra com-

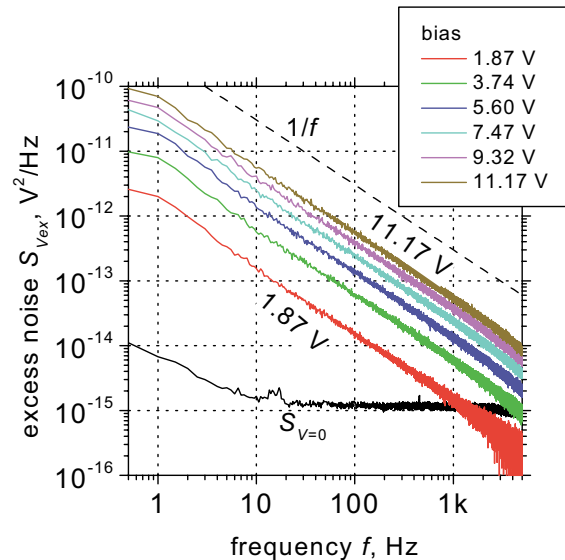


Fig. 2. Excess noise of sample P-120 at several bias voltages (listed in the legend)

Rys. 2. Szum nadmiarowy rezystora P-120 zmierzony przy różnych napięciach polaryzacji

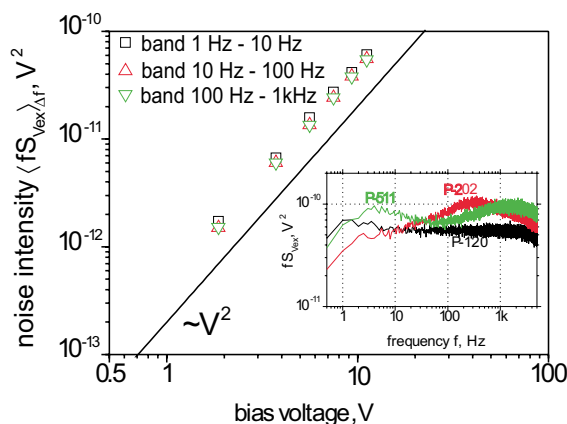
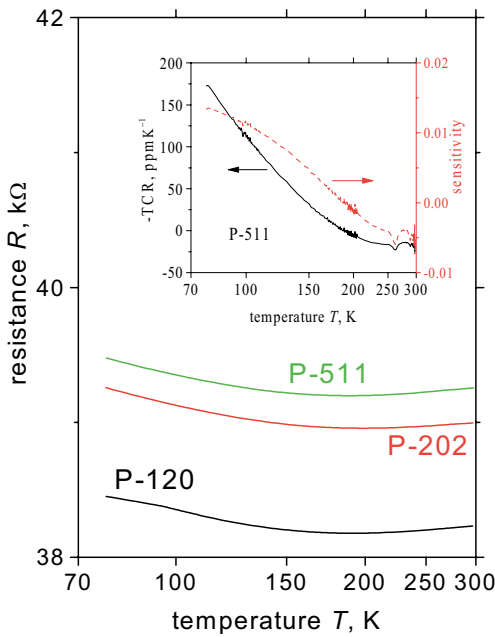


Fig. 3. Noise intensity in different frequency bands vs. sample bias voltage, calculated for data from figure 2. In the inset: product of excess noise and frequency for different TFRs plotted vs. frequency to emphasize spectra components other than  $1/f$   
Rys. 3. Intensywność szumu wyznaczona w różnych pasmach częstotliwości, wykreślona w funkcji napięcia polaryzacji dla rezystora P120. We wstawce: iloczyn szumu nadmiarowego i częstotliwości wykreślony w funkcji częstotliwości

ponents other than  $1/f$  noise. It is more pronounced in such graph that for samples P-202 and P-511 apart from  $1/f$  noise also Lorentzians exist.

### Temperature dependence of resistance

Further studies were performed during slowly varying temperature. Temperature dependence of resistance is shown in *Fig. 4*. Using  $R(T)$ , temperature coefficient of resistance (TCR) has been calculated and plotted in the inset of *Fig. 4*. Since granular materials, like  $\text{RuO}_2$ , gain win recognition in the field of temperature sensors for low temperature range, another useful parameter for comparison properties of different temperature sensors has also been evaluated. Dimensionless sensitivity,  $A \equiv (T/R)|dR/dT|$ , has been calculated and added to plot in the inset of *Fig. 4*. Sensitivity for typical low-temperature sensors reaches the value of order of 1 or more in studied temperature range, while for  $\text{RuO}_2/\text{CaRuO}_3$ -based TFRs it is two orders of magnitude smaller.



**Fig. 4. Temperature dependence of resistance. Temperature coefficient of resistance (solid line) and dimensionless sensitivity (dashed line) are shown in the inset**

**Rys. 4. Temperaturowa zależność rezystancji. We wstawce temperaturowy współczynnik rezystancji (linia ciągła) i czułość bezwymiarowa (linia przerywana)**

### Low-frequency noise spectroscopy

Since size effect evaluated with the use of ordinary voltage measurements is close to ideal value (see *Table 1*), noise measurements had to be involved in order to obtain the knowledge about (i) the quality of resistive-to-conductive films interface and (ii) noise properties of resistive material. Noise in studied samples has been identified to be resistance noise, therefore bias independent PSD of resistance fluctuations,  $S_R = S_{vex}(f)/R^2$ , has been used in noise maps. Noise maps are contour graphs of the product  $fS_R$  vs. frequency and reciprocal temperature. They have been obtained for different sectors of TFRs (i.e. parts of the main film spanned between two voltage probes) by the use of cross-correlation method [6]. Exemplary maps, measured simultaneously on different sectors of TFRs, are shown in *Fig. 5*. Thermally activated noise sources (TANSs) are visible as streaks on maps. Their slope relates to activation energy  $E_a$  of TANS [7, 8]. Set of TANSs is sample-specific rather than material-specific.

There are TANSs visible on the noise map of *Fig. 5a* that are not detected on map in *Fig. 5b*. Thus, these TANSs are located beyond the sector 6–7 of TFR. Hence, noise maps are also helpful in spatially localization of TANSs. Another interesting phenomenon visible on map of *Fig. 5b* is spectra switching [8] that takes place at 270 K and 180 K, where TANSs with activation energy 0.52 eV and 0.26 eV (respectively) switch on/off. One should note however, that the map of *Fig. 5b* concerns the most outer sector (6–7), including conductive-to-resistive film interface. No spectra switching has been observed in samples P-120 and P-202.

### Noise scaling

The intensity of all noise sources in one sector of TFR can be calculated as the power of resistance fluctuations  $\langle \delta R^2 \rangle$ . Since noise maps are sample-specific,  $\langle \delta R^2 \rangle(T)$  dependencies are also different, even for TFRs prepared from the same resistive paste. Hence, integral measure of noise [9]

$$s_T \equiv \frac{1}{T_2 - T_1} \int_{T_1}^{T_2} \int_{f_l}^{f_u} S_R(f, T) df dT, \quad (1)$$

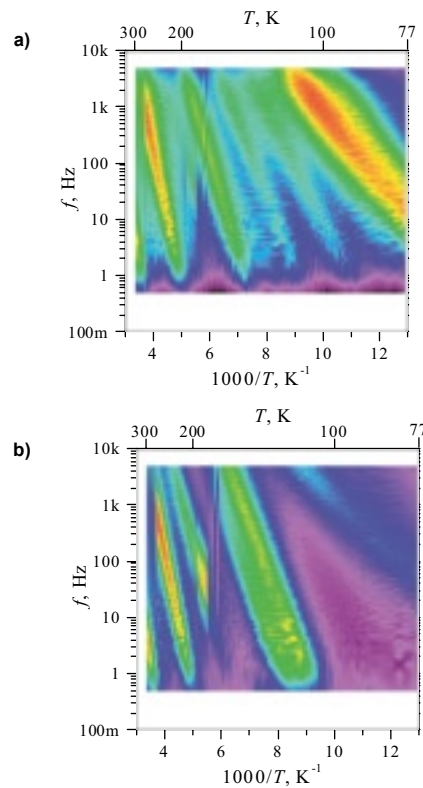


**Fig. 5. Noise maps for sample P-511 measured on sectors 1-7 (a) and 6-7 (b)**

**Rys. 5. Mapy szumowe wyznaczone dla rezystora P-511 na sektorach 1-7 (a) i 6-7 (b)**

where  $T_1 = 77$  K and  $T_2 = 300$  K, has been involved to obtain reliable noise measure for noise properties comparison of various TFRs.

Using voltages acquired from different voltage terminations in cross-correlation method it is possible to study noise vs. volume of the resistive film. The method and its advantages have been discussed in [6]. Bulk and contact noise components have been extracted from linear dependence of integral  $s_T$  on sector volume, what has been illustrated in *Fig. 6*. Bulk noise per square,  $s_{sq}$ , is calculated as the slope of the lines drawn trough points corresponding internal TFRs sectors. Next, dimension-independent bulk noise intensity  $C_{bulk}$  is obtained,  $C_{bulk} \equiv s_{sq} / \Omega_{sq}$ , where  $\Omega_{sq} = dw^2$  is the volume of the individual square. Parameter  $C_{bulk}$  is often used for comparison noise properties of different materials. On the other hand, difference between integral  $s_T$  calculated for total resistor  $s_{T(1-7)}$  and extrapolated bulk noise  $s_{bulk} = L/w \times s_{sq}$ , gives contact noise  $s_{int}$ :  $2s_{int} \equiv s_{1-7} - s_{bulk}$ . It leads to contact-geometry-independent parameter  $C_{int} \equiv ws_{int}/s_{sq}$  [9]. The value of  $C_{int}$  corresponds to the hypothetical length of the resistive film which has the noise equal the interface noise. Calculated values of  $C_{bulk}$  and  $C_{int}$  are listed in *Table 2*.

**Tabl. 2. Noise parameters of Pb/Cd-free CaRuO<sub>3</sub>-based TFRs calculated from noise scaling**

**Tab. 2. Parametry szumowe bezołowiowych rezystorów z RuO<sub>2</sub>/CaRuO<sub>3</sub> wyznaczone na podstawie skalowania szumu**

Sample	P-120	P-202	P-511
$C_{bulk} \cdot 10^{24}, m^3$	229	324	368
$C_{int}, mm$	1.4	0	1.5
$K \cdot 10^{21}, m^2/\Omega$	3.7	5.1	5.7

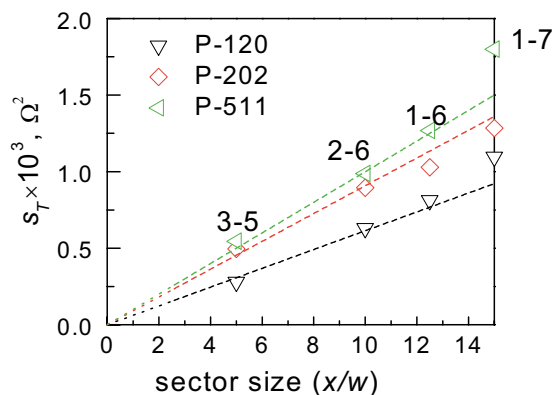


Fig. 6. The integral  $s_T$  (points) vs. sector size. Sectors are labeled near most upper corresponding markers

Rys. 6. Całka  $s_T$  (punkty) w funkcji rozmiaru sektora rezystora. Obok punktów podane są identyfikatory sektorów dla których wyznaczono wartości  $s_T$ .

### Noise of resistive film

Bulk noise of TFRs is proportional to resistivity  $\rho$ ,  $C_{bulk} = K'\rho$ , when resistivity is changed by the content of conductive constituent of the resistive paste [10–12]. The value  $K' = 2 \cdot 10^{-20} \text{ m}^2 \Omega^{-1}$  has been obtained for Pb/Cd-free  $\text{CaRuO}_3$ -based sample "P-202 Sz R-10-73,5  $\text{CaRuO}_3$ ", examined in [6]. However, the value of  $K'$  for currently studied samples, made from new resistive  $\text{RuO}_2/\text{CaRuO}_3$ -based paste, is nearly an order of magnitude smaller (see table 2) and is close to  $K' = 2 \cdot 10^{-21} \text{ m}^2 \Omega^{-1}$  for Pb/Cd-free  $\text{RuO}_2$ -based TFRs [6] or Pb-containing  $\text{BiRu}_2\text{O}_7$ -based TFRs [9] but it is still larger than  $K' = 4 \cdot 10^{-22} \text{ m}^2 \Omega^{-1}$  for Pb-containing  $\text{RuO}_2$ -based TFRs [9].

### Summary

Innovative conducting component has been used for preparation Pb/Cd-free resistive paste, which is the mixture of  $\text{CaRuO}_3$  and  $\text{RuO}_2$  powders of controlling ratio. TFRs made of it with different contacts, were studied in temperature range 77...300K.  $R(T)$  dependence has minimum at 190 K and  $|\text{TCR}| < 200 \text{ ppm/K}$ . Dimensionless sensitivity is less than 0.15, what excludes application in temperature sensing.

Two basic components of low-frequency excess noise have been revealed, both originated from resistance fluctuations. Apart from  $1/f$  noise, also Lorentzians exist, resulting from TANSs. TANSs with activation energy in the range 0.08 eV – 0.6 eV have been detected on noise maps obtained by the use of low-frequency noise spectroscopy. For sample with Ag-AgPt-Pd contacts, spectra switching has been observed for TANSs located in the sectors of TFRs adjacent the current contacts.

Two noise components have been extracted from the whole TFRs noise: (i) bulk noise intensity  $C_{bulk}$  and (ii) describing interface noise  $C_{int}$ . The values of  $C_{bulk}$  have been found to be

in the range from  $2 \cdot 10^{-22}$  to  $4 \cdot 10^{-22} \text{ m}^3$ , what means significant improvement with respect to (also Pb/Cd-free)  $\text{CaRuO}_3$ -based TFRs studied in [6], where  $C_{bulk} = 8.6 \cdot 10^{-21} \text{ m}^3$ .

Size effect calculated from ordinary resistance measurements was negligible. Hence, noise measurements were involved in quality of the conductive-to-resistive films interface examination, by the use of  $C_{int}$  parameter. The values of  $C_{int}$  (see table 2) have been found to be close to that obtained in [6] and [9]. Thus, Ag and AgPd conducting pastes form good interface with new  $\text{RuO}_2/\text{CaRuO}_3$ -based resistive paste. In the case of Ag-AgPt-Pd contacts, the value of  $C_{int}$  is satisfactory, however spectra switching is possible in the interface region, what might degrade usefulness in high-reliability applications.

The work has been supported by grant no N N515 341836 from Polish Ministry of Science and Higher Education, and Rzeszow University Project no U7371/DS.

### References

- [1] Morten B., Ruffi G., Sirotti F., Tombesi A., Moro L., Akomolafe T.: Lead-free ruthenium-based thick-film resistors: a study of model systems. *Journal of Materials Science: Materials In Electronics* 2, 1991, 46–53.
- [2] Jakubowska M.: Thick Film Materials – Achievements and Trends in Development. Proc. of 32nd Int. Conf. of IMAPS – CPMT IEEE Poland, Pułtusk, 2008.
- [3] Prudenziati M., Zanardi F., Morten B., Gualtieri A.F.: Lead-free thick film resistors: an explorative investigation. *Journal of Materials Science-Materials in Electronics* 13, 2002, 31–7.
- [4] Rane S., Prudenziati M., Morten B., Golonka L., Dziedzic A.: Structural and electrical properties of perovskite ruthenate-based lead-free thick film resistors on alumina and LTCC. *Journal of Materials Science: Materials in Electronics* 16, 2005, 687–691.
- [5] Maeder T., Jacq C., Grimaldi C., Ryser P.: Lead-free low-firing thick-film resistors based on bismuth glasses and ruthenium oxide. Proc. of 33rd Int. Conf. of IMAPS Poland Chapter (Poland, Gliwice), 2009.
- [6] Stadler A.W., Kolek A., Zawiślak Z., Mleczo K., Jakubowska M., Kielbasiński K.R., Młodziński A.: Noise properties of Pb/Cd-free thick film resistors. *J. Phys. D: Appl. Phys.* 43, 2010, 265401.
- [7] Kolek A., Stadler A.W., Ptak P., Zawiślak Z., Mleczo K., Szalański P., Żak D.: Low-frequency  $1/f$  noise of  $\text{RuO}_2$ -glass thick resistive films. *J. Appl. Phys.* 102, 2007, 103718.
- [8] Kolek A., Stadler A.W., Zawiślak Z., Mleczo K., Dziedzic A.: Noise and switching phenomena in thick-film resistors. *J. Phys. D: Appl. Phys.* 41, 2008, 025303.
- [9] Mleczo K., Zawiślak Z., Stadler A.W., Kolek A., Dziedzic A., Cichosz J.: Evaluation of conductive-to-resistive layers interaction in thick-film resistors. *Microelectronics Reliability* 48, 2008, 881–5.
- [10] Vandamme L.K.J.: Criteria of Low-Noise Thick-Film Resistors. *ElectroComp. Sci. Technol.* 4, 1977, 171–7.
- [11] Wolf M., Müller F., Hemschik H.: Comment on the dependence of  $R_{\square}$  and current noise on grain size in thick film resistors – TFR's. *Active and Passive Elec. Comp.* 12, 1985, 59–61.
- [12] Müller F., Wolf M.: Dependence of the Sheet Resistivity and Current Noise Behaviour of the Grain Size and Volume Fraction of Conducting Material in Thick-Film Resistors Experiments. *Active and Passive Elec. Comp.* 13, 1988, 1–6.